Humidity-Driven Supercontraction and Twist in Spider Silk

Noy Cohen*
Department of Materials Science and Engineering, Technion—Israel Institute of Technology, Haifa 3200003, Israel

Claus D. Eisenbach
Materials Research Laboratory, University of California, Santa Barbara, California 93106, USA and Institute for Polymer Chemistry, University of Stuttgart, D-70569 Stuttgart, Germany

(Received 7 June 2021; revised 5 January 2022; accepted 9 February 2022; published 28 February 2022)

Spider silk is a protein material that exhibits extraordinary and nontrivial properties such as the ability to soften, decrease in length (i.e., supercontract), and twist upon exposure to high humidity. These behaviors stem from a unique microstructure in combination with a transition from glassy to rubbery as a result of humidity-driven diffusion of water. In this Letter we propose four length scales that govern the mechanical response of the silk during this transition. In addition, we develop a model that describes the microstructural evolution of the spider silk thread and explains the response due to the diffusion of water molecules. The merit of the model is demonstrated through an excellent agreement to experimental findings. The insights from this Letter can be used as a microstructural design guide to enable the development of new materials with unique spiderlike properties.

DOI: 10.1103/PhysRevLett.128.098101

Spider silk is a high performance biomaterial with outstanding mechanical properties that are based on their hierarchically structured morphology [1–5]. Phenomenologically, spider silk is a multiphase system comprising a crystalline and amorphous phase, where crystalline domains of stacked poly (alanine) β sheets are dispersed in an anisotropic amorphous polypeptide matrix. Crystalline β-sheet domains are interconnected by highly aligned and extended glycine-rich polypeptide segments [4,6]. The matrix in which β-sheet domains are embedded is often referred to as "semi-amorphous" because, in addition to fully amorphous random-coil regions, it comprises less orderly (single) β structures, 3_1 helices, and β turns [7]. The multiphase morphology results from the segmented structure of the polypeptide chains, comprising highly crystallizable longer alanine sequences in an otherwise comparatively randomly and short sequenced polypeptide chain with a tendency towards mesophase formation [4]. The main components of dragline silk are the major ampullate spidroin protein 1 (MaSP1) and the major ampullate spidroin protein 2 (MaSp2), which are characterized by molecular weights of ~250 and ~350 kDa, respectively [8]. Typically, β-sheet nanocrystalline domain sizes are $2 \times 3 - 5 \times 7$ nm [intersheet, interchain (hydrogen bond), and fiber (chain axis) direction], with interdomain distances of ~14 nm along the chain axis [6,9]. Dimensions vary between spider and silkworm silk, and may significantly differ even within one type of silk, e.g., silkworm fiber [10].

In the naturally spun silk thread, both β-sheet crystallites and polypeptide chains in the semi-amorphous phase are oriented along the preferred fiber direction [4,6]. The high fiber orientation results from the spinning process that includes an intermediate liquid-liquid phase separation under the formation of a lyotropic liquid crystalline (LC) phase, followed by increasing molecular alignment as the spinning dope is concentrated by loss of water during the ion exchange in the tapering spinning duct, finally causing a liquid-solid phase transition [11–13]. When the dope has exited the spinneret, residual water is lost by evaporation in air and vitrification of the silk fiber takes place [11]. This means fixation of the silk fiber orientation, given its high glass transition temperature $T_g \sim 200\,^{\circ}\mathrm{C}$ [14].

A characteristic feature of the silk thread is its fibril-like structure, as revealed by SAXS [9,15,16], SANS [17], microscopy [18], SEM [9,16,18], and AFM [3,9,15,16,19] investigations. These studies showed that the silk thread consists of bundled strains of nanofibrils which comprise granules that are molecularly interconnected and aligned along the fiber axis, with the spidroin chains lying parallel to the long axis. In this context, it has to be emphasized that the individual fibrils resembling features are not crystalline but highly oriented LC domains that have been frozen in the glassy state. The only crystalline features are the assemblies of β sheets that act as multifunctional cross-links (and fillers). The molecularly interconnected fibrils are part of the hierarchical structure and comprise the multiphase morphology described above. Depending on the spider species and the analysis method applied, dimensions of individual (nano-)fibrils may vary between 35 to 150 nm in diameter and 100 to 500 nm in length. Accordingly, the

silk thread comprises hundreds of fibrils per cross section of diameter ~3–7 μm.

Interestingly, it follows from early light microscope observations [18] and AFM results [3] that dragline silk thread consists of spirally twisted fibrils (see Supplemental Material [20], Sec. S1).

One of the unusual properties of spider dragline silk thread is supercontraction, i.e., the significant shortening of up to ~60% in length upon the wetting of unrestrained fibers as a result of an increase in the environmental relative humidity (RH) [21–23]. This phenomenon results from the transition of a highly oriented glassy phase to a disordered rubbery phase [24–27]. The driving force is the gain in conformational entropy of polypeptide segments connecting crystalline β-sheet domains as the semiamorphous phase turns from glassy to rubbery. In other words, extended chains adopt a random coil conformation during this transition. Recently, we have derived a microscopically motivated and energy-based model that captures the underlying mechanisms that give rise to supercontraction [28].

Another unique behavior of spider dragline silk thread recently observed in a specially designed experiment is a humidity-induced torsional deformation of the naturally spun silk thread [29]. In a torsion pendulumlike apparatus [30,31], a silk thread (~90–120 mm in length and ~3–7 μm in diameter) is fixed at one end and a ring-shaped paddle weight (~0.1 g) is attached at the freely dangling end. The pendulum is enclosed with a humidity cabinet that allows for a controlled RH change of the environment. The humidity-induced twist deformation of the fiber is measured from the rotation motion of the attached mass recorded with a video camera. Above a threshold RH of ~70%, a torsional response of the freely hanging silk thread between 130–350 °/mm was observed, corresponding to 30–85 full 360° rotations of the dragline silk thread around its axis. The authors propose that this behavior results from structural relaxation that is made possible by the humidity-driven glass-rubber transition. Based on molecular simulations at the protein level, the phenomenon has been related to a transition of straight proline containing segments to a twisted form in MaSp2. As admitted by the authors [29], this explanation is not to exclude the possibility of larger-scale mechanisms.

In this Letter, we derive a model that accounts for the macroscopic structure and morphology of the entire dragline silk fiber, consisting of an ensemble of helically interwinded silk strands, and captures the supercontraction as well as the twist phenomena.

The similarities between the dependency of the supercontraction and the twist of spider dragline silk on RH infer a common underlying mechanism. Experiments show that a threshold RH that enables a transition from a continuous glassy to a rubbery phase has to be reached before a mechanical response is observed. The reported critical RH value is around 70% for both the supercontraction [25,32,33] and the twist [29] response, which require the presence of a rubbery phase and are related to single chain conformational entropy features. Phenomenologically, the reaching of a rubbery state is the only essential requirement for the supercontraction of dragline spider silk, which is solely driven by entropic elasticity of polymer chains in the melt. In contrast to this, the rubbery state is a necessary, but not a sufficient precondition for the observation of a torsional deformation in spider dragline silk. Rotation of the silk thread under tension around its axis cannot be explained by a molecular level mechanism as feasible for supercontraction, but has to include the macroscopic structure—helically interwinded fibrillar strands [3,18]—and their humidity-induced softening and subsequent untwisting.

Above the critical RH, the vanishing of the macroscopic helical features alone would cause an extension of the silk thread. However, this is counteracted by elastically active polypeptide segments in rubbery domains. Whether the dragline silk specimen elongates or shrinks during the transition of the continuous semi-amorphous phase from glassy to rubbery depends on the weight of the paddle attached at its free end. The fact that an extension of the sample of only about 1.5% after the test was observed [29] shows that the tension from the paddle prevented elastically active chain segments between crystalline β-sheet domains from staying in the extended chain conformation (as in the glassy silk fiber) but allowed some decrease in their end-to-end distance by partial coiling. Thus, the longitudinal contraction is constrained from the paddle [29].

Considering the length of the shape-anisotropic fibrils, which may vary between 100–500 nm, and taking into account the experimentally measured maximum rotation per unit length, which varies between 130–350 °/mm, we approximate a relative twist 0.013°–0.185° between individual fibrillary objects. A similar approach to the hypothetical twisting of fully extended spidroins gives about 0.16°–0.46° against each other, at most. The latter figure is based on an average spidroin molecular weight of 300 kDa, translating to polypeptide chains comprising 3500 monomer repeat units with an average molecular weight of 88 Da. Taking a contour length ~0.35 nm per monomer repeat unit, the length of a fully extended spidroin is ~1.2 μm. These calculations show that the twisting is extremely small on a molecular scale, but has an enormous effect on the macroscopic behavior.

Following the above analysis, we distinguish between different length scales in the dragline silk. In the glassy and the transient state, the silk is characterized by four length scales [Figs. 1(a) and 1(b)]. The first is a nanoscale with typical dimensions of nm that includes the polypeptide chains and the β sheets. The mesoscale includes nanofibrils with typical dimensions of 10–10^3 nm [Figs. 1(a) and 1(b), top] that are made from aggregates of polypeptide chain segments (highly aligned in the glassy state, and of

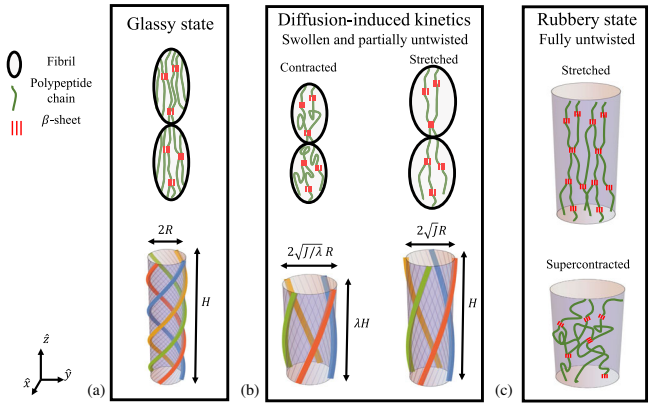

FIG. 1. Structure model of spider dragline silk; four helical fibrillar strands are highlighted in color for clarity. (a) Glassy state of natural dry fiber; (b) transient states during water absorption showing a contracted and a twisted thread (clockwise torsion); (c) fully rubbery state.

decreasing intermolecular correlation as water diffuses into the fiber) and stacked β sheets. The third length scale is microscopic and characterized by a helical fiber made from a helical arrangement of nanofibrils in series. The macroscale is the dragline silk thread that comprises an interconnected and intertwined assembly of helical fibrillar strands.

In the fully rubbery state, there are no hydrogen bonds that connect the polypeptide chains in the formerly semiamorphous phase or any features reminiscent of fibrils. This structure can be described by two length scales [Fig. 1(c)]: (i) the nanoscale, comprising polypeptide chains [coiled in the supercontracted state, Fig. 1(c) bottom] which are cross-linked by β sheets domains, and (ii) the macroscale, pertaining to the complete dragline silk.

As illustrated in the work of Cohen *et al.* [28], the supercontraction effect occurs and is dominant in all scales. Specifically, this phenomenon stems from the entropy gain and the loss of orientation of the individual chains and the nanofibrils. The twist motion, however, is associated with microscopic and macroscopic changes, including (i) the humidity-induced softening (glass-rubber transition), (ii) the untwisting of strands of nanofibrils, and (iii) the simultaneous gain of conformational entropy in rubbery polypeptide chain segments.

Below a critical RH, the water concentration in the silk fiber is not high enough for lowering its glass transition temperature T_g below the ambient temperature [21,32]. It is only at and beyond this critical RH that glassy phase turns rubbery. In the proposed semimicroscopic model, as water diffuses into the silk thread, the formation of rubbery domains growing from the surface into the fiber is random. Eventually, radial percolation of the rubbery phase in the silk thread interrupts the original longitudinal continuity of the all-glassy phase. This marks the onset of the observed mechanical response (torsion or contraction). As water uptake increases, the rubbery phase grows at the expense of the glassy phase, causing further deformation. We anticipate that the penetration of water molecules is enabled as long as the RH is maintained (or increases) above a critical value. Once all the hydrogen bonds dissociate, the humidity-driven response ends [28].

To model the kinematics of dragline silk, we consider a thread in its dry glassy state with radius R_o and length H that comprises a helical arrangement of intertwining bands of nano—or microfibrils [Fig. 1(a)] [3,18]. The average helical strand has α_0 turns per unit referential length. At time $t = 0$, the volume fraction of water molecules in the thread $c(t = 0) \approx 0$, the RH increases beyond the critical value (of ~70%), and a transition process from a glassy to a rubbery state begins.

Because of the water uptake, the length, the radius, the volumetric deformation, and the number of turns per unit length in the silk thread at time $0 \le t$ are $h_{sc}(t) = \lambda_{sc}(t)H$, $r_{sc}(t, R) = \sqrt{J_{sc}(t)/\lambda_{sc}(t)}R$, $J_{sc}(t) = 1/(1 - c(t))$, and $\alpha_{sc}(t)$, respectively. The radius of the thread by $\bar{r}_{sc} = r_{sc}(t, R_o)$. We refer to the configuration at time t as the hydrated traction-free state and define a polar coordinate system in which the fiber is along the $\hat{\mathbf{z}}$ direction such that the deformation gradient from the dry to the hydrated traction-free state is (see Sec. S2 in the Supplemental Material [20])

$$\mathbf{F}_{sc}(t) = \begin{pmatrix} \sqrt{\frac{J_{sc}}{\lambda_{sc}}} & 0 & 0 \\ 0 & \sqrt{\frac{J_{sc}}{\lambda_{sc}}} & r_{sc}\alpha_{sc} \\ 0 & 0 & \lambda_{sc} \end{pmatrix}. \tag{1}$$

We focus on the region $0 \le c(t) \le \tilde{c}$, where $\tilde{c}$ is the amount of water that is required to dissociate all of the hydrogen bonds in the thread [34,35]. Considering the density of dry silk is ~1.3 g/cm^3 and an average molecular weight of the spidroin's repeat unit of 88 Da, we obtain $\tilde{c} \approx 0.21$ and $J(\tilde{c}) \le 1.27$.

Experimental evidence reported in literature [29,33] shows that the strain or the twist roughly depend on $\sqrt{t}$, thereby suggesting that water is diffused into the silk over time. We emphasize that the number of dissociated hydrogen bonds and the decrease in T_g is proportional to c [32,36,37]. This infers that the diffusion of water molecules into the thread governs the supercontraction and the twist response. As an approximation, we assume that this process follows Fick's law [38] such that the volume fraction of water in the thread is

$$c(t) = k\sqrt{t}, \tag{2}$$

where k is a constant that accounts for the diffusion coefficient, the geometry of the fiber, the maximum amount

of water that can be absorbed, and the rate of RH increase [39]. We point out that the water content c is related to the RH through k.

The stretch and the number of turns per unit length in the helical features of the thread depend on $c(t)$. As a first order approximation in c, we set

$$\lambda_{sc}(c) = 1 - \frac{c}{\tilde{c}}(1 - \lambda_m), \tag{3}$$

$$\alpha_{sc}(c) = \left(1 + \frac{c}{\tilde{c}}\right)\alpha_0, \tag{4}$$

where $\lambda(\tilde{c}) = \lambda_m$ is the stretch in the fully supercontracted state and $\alpha(\tilde{c}) = 0$. In this state, all the hydrogen bonds have been dissociated and the silk thread is fully rubbery, as shown in Fig. (1c). Note that substitution of Eq. (2) into Eqs. (3) and (4) allows to write $\lambda_{sc}(t)$ and $\alpha_{sc}(t)$.

Next, a load is applied to the silk thread. As a result, the length and the radius with respect to the dry state are $h = \lambda H$ and $r = \sqrt{J_{sc}/\lambda}R$, respectively, and the average helical strand has α turns per unit length. We refer to this configuration as the hydrated loaded state. The deformation gradient $\mathbf{F}$ from the dry to the hydrated loaded state is given by substitution of λ_{sc}, r_{sc}, and α_{sc} with λ, r, and α, respectively, in $\mathbf{F}_{sc}$ [Eq. (1)] (see Sec. S2 in the Supplemental Material [20]).

To model the nonlinear constitutive response of a thread with a fixed water content at time t, we assume that the spider silk is hyperelastic and the water molecules and the protein network are incompressible. We define the energy density function $\psi = E/6\mathrm{Tr}[\mathbf{F}_{sc}^{-T}(\mathbf{F}^T\mathbf{F} - \mathbf{I})\mathbf{F}_{sc}^{-1}]$, where $\mathrm{Tr}(\bullet)$ denotes the trace of the tensor $\bullet$ and $E(c)$ is the Young's modulus, which depends on the water content in the thread [21,28,32]. In this Letter, we propose the relation $E(c) = E_G/(1 + \gamma c)$, where E_G is the Young's modulus in the dry glassy state and γ is a constant that accounts for the softening. Note that the Young's modulus in the rubber state is given by $E(c = \tilde{c})$. This expression agrees with experimental findings, as shown in Sec. S3 of the Supplemental Material [20].

The true stress tensor can be derived from the energy density function via $\boldsymbol{\sigma} = (\partial\psi/\partial\mathbf{F})\mathbf{F}^T = E/3\mathbf{F}\mathbf{F}_{sc}^{-1}\mathbf{F}_{sc}^{-T}\mathbf{F}^T - \Pi\mathbf{I}$. Here, Π is a workless pressurelike term stemming from the incompressibility determined from the boundary conditions. Following the available experimental data, we set the radial stress component $\sigma_{rr} = 0$ and determine the stress. Consequently, the force and the torque that develop in the thread are (see Sec. S4 in the Supplemental Material [20])

$$F = \frac{E}{3}\left[\frac{\lambda}{\lambda_{sc}} - \left(\frac{\lambda_{sc}}{\lambda}\right)^2\right]A, \tag{5}$$

$$T = \frac{E}{3\lambda}I_p(\alpha - \alpha_{sc}), \tag{6}$$

respectively, where $A = \pi\bar{r}_{sc}^2$ and $I_p = \pi\bar{r}_{sc}^4/2$ are the cross-sectional area and the polar moment of inertia of the hydrated traction-free thread. Once the boundary conditions are prescribed in terms of F and T, Eqs. (5) and (6) can be used to determine the stretch λ and the twist per unit length α.

To illustrate the merit of the model, we compare its predictions to experiments on two spider genera—*Argiope* and *Nephila* [29,33]. To this end, we reconstruct the data such that supercontraction or twist begin at $t = 0$ and set $\lambda_m = 0.86$ [33], $\tilde{c} = 0.21$, and, considering the conflicting data on Young's modulus [32,40–44], $E_G = 10$ GPa. The values of k, α_0, and γ are fitted to experimental data.

Figures 2(a) and 2(b) plot the fit of the supercontraction in Eq. (3) and the supercontraction stress to the measurements of Giesa *et al.* [33] and Agnarsson *et al.* [39] on *N. Clavipes*, respectively. We offset the times by $t = 30$, 10, and 5 mins such that all experiments begin at $t = 0$. In addition, the experiments of Agnarsson *et al.* [39] introduced an initial load of ~20 MPa to ensure the silk thread is taut. To enable comparison, we subtract this initial load and only plot the RH-driven stress.

In the experiment of Giesa *et al.* [33], we set $F = 0$ and find that $\lambda = \lambda_{sc}$. To capture the longitudinal stress, we prescribe $\lambda = 1$ and plot $P = F/(\pi R_o^2)$ [Eq. (5)]. The experiments performed by Agnarsson *et al.* [39] investigated the influence of the rate of RH increase on the overall response. We point out that as water penetrates the thread, two contradicting phenomena occur: (i) the thread wants to supercontracts, thereby giving rise to an increase in stress and (ii) a significant softening is achieved. The net result is a stress build up which saturates once the two mechanisms counteract each other. The overall response is governed by the rate of RH increase through the reduction in E and the diffusion related constant k. Our model is capable of capturing the experimental results by fitting $\gamma = 40$ and $k = 2.5 \times 10^{-3}$ min^{-1} for the slow RH increase and $k = 0.02$ min^{-1} for the fast RH increase rate.

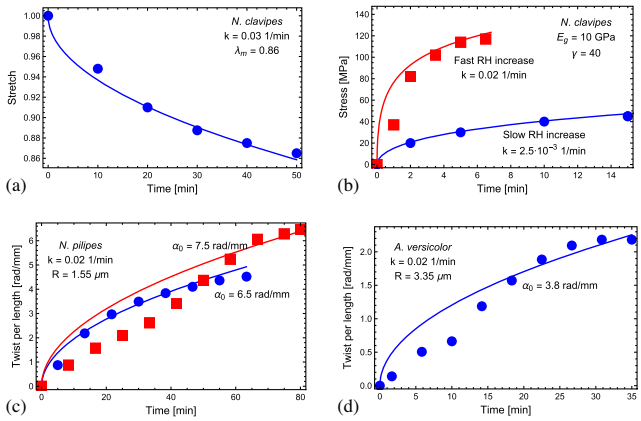

FIG. 2. Comparison of the model predictions (continuous lines) to experimental findings (circle and square marks). (a) Supercontraction [33] and (b) supercontraction stress [39] that develop in *N. Clavipes*. Twist of (c) *N. pilipes* and (d) *A. versicolor* [29].

Figures 2(c) and 2(d) demonstrate the ability of the model to capture the twist per unit length of *N. pilipes* and *A. versicolor*, respectively, as measured by Liu *et al.* [29]. The times are offset by $t \approx 4$, 8.5, and 7 mins for *N. pilipes* and *A. versicolor*, respectively. Here, we prescribe $F = f_0$ and $T = 0$ in Eqs. (5) and (6), where $f_0 = 0.98$ mN is the force due to the weight of the paddle that was used in the experiment, and solve for $\lambda(t)$ and $\alpha(t)$. The fitting parameters are shown in the plot.

Recall that the parameter α_0 is the average number of turns per unit length and measures the initial helicity of the thread. Thus, we conclude that the microstructure of threads from *N. pilipes* are more helical than those in *A. versicolor*. In addition, the similarities in the value of the k parameter suggests that the diffusion process into the three silk threads is similar.

Interestingly, Fig. 2(c) and the findings of Liu *et al.* [29] highlight the problem of getting reproducible results in biological materials produced by living organisms. This is evident from the twisting behavior of two *N. pilipes* samples, i.e., from the same kind of spider silk, reported in Ref. [29]. In that work, Fig. (3A) shows a smooth increase in twist while Fig. (S2) is characterized by an inflection point. It is noted that the latter behavior is observed when the angular speed experienced significant fluctuations (inset in Fig. (S2) as compared to Fig. (3B) of Ref. [29]). This is also the case for *A. versicolor*, where the deviations in the curve progression of the twist per unit length seen in Fig. 2(d) correlate with the observation of angular speed fluctuations (Fig. (3D) in Ref. [29]). This further sheds light on this problem.

It is also worth mentioning that Liu *et al.* [29] reported that the silk threads experienced a slight elongation (of $\sim$1.5%) during the experiment. This effect stems from two factors: (i) the weight of the paddle and (ii) the softening due to water uptake. While experimental data that record the extension over time are not available, we show that our model is capable of capturing the experimentally observed range of elongations, as described in Sec. S5 in the Supplemental Material [20].

The good to excellent agreement of our model with experimental data on supercontraction and twist of dragline silk from three different spider species and two genera clearly demonstrate its validity.

In conclusion, this Letter introduces a microscopically motivated structural model for spider silk that is capable of explaining the kinematic evolution and the constitutive behavior that stem from humidity-driven diffusion of water. In particular, the macroscopic torsion observation is due to untwisting of helical fibril structures which allow for conformational changes of spidroins on the nanoscopic scale, and thus for gain in conformational entropy when transitioning from the glassy to rubbery state. In addition, a simple analytical model is derived based on the structural model to quantitatively estimate the transient behavior of supercontraction and twist. Our proposed framework is in agreement with various experimental findings. The insights from this Letter can be used to guide the design of new biologically inspired materials.

This work was supported in part by the National Science Foundation Materials Research Science and Engineering Center (IRG-3) DMR 1720256.

*noyco@technion.ac.il

[1] F. Vollrath, Strength and structure of spiders silks, Rev. Mol. Biotechnol. **74**, 67 (2000).
[2] L. Roemer and T. Scheibel, The elaborate structure of spider silk: Structure and function of a natural high performance fiber, Prion **2**, 154 (2008).
[3] G. Xu, L. Gong, Z. Yang, and X. Y. Liu, What makes spider silk fibers so strong? From molecular-crystallite network to hierarchical network structures, Soft Matter **10**, 2116 (2014).
[4] T. Lefevre and M. Auger, Spider silk as a blueprint for greener materials: A review, Int. Mater. Rev. **61**, 127 (2016).
[5] J. L. Yarger, B. R. Cherry, and A. van der Vaart, Uncovering the structure-function relationship in spider silk, Nat. Rev. Mater. **3**, 18008 (2018).
[6] J. D. van Beek, S. Hess, F. Vollrath, and B. H. Meier, The molecular structure of spider dragline silk: Folding and orientation of the protein backbone, Proc. Natl. Acad. Sci. U.S.A. **99**, 10266 (2002).
[7] S. Keten and M. J. Buehler, Nanostructure and molecular mechanics of spider dragline silk protein assemblies, J. R. Soc. Interface **7**, 1709 (2010).
[8] W. A. Gaines IV and W. R. Marcotte, Jr., Identification and characterization of multiple Spidroin 1 genes encoding major ampullate silk proteins in Nephila clavipes, Insect molecular biology **17**, 465 (2008).
[9] N. Du, X. Y. Liu, J. Narayanan, L. Li, M. L. M. Lim, and D. Li, Design of superior spider silk: From nanostructure to mechanical properties, Biophys. J. **91**, 4528 (2006).
[10] C. Guo, J. Zhang, X. Wang, A. T. Nguyen, X. Y. Liu, and D. L. Kaplan, Comparative study of strain-dependent structural changes of silkworm silks: Insight into the structural origin of strain-stiffening, Small **13**, 1702266 (2017).
[11] F. Vollrath and D. P. Knight, Liquid crystalline spinning of spider silk, Nature (London) **410**, 541 (2001).
[12] M. Heim, D. Keerl, and T. Scheibel, Spider silk: From soluble protein to extraordinary fiber, Angew. Chem., Int. Ed. Engl. **48**, 3584 (2009).
[13] T.-Y. Lin, H. Masunaga, R. Sato, A. D. Malay, K. Toyooka, T. Hikima, and K. Numata, Liquid crystalline granules align in a hierarchical structure to produce spider dragline microfibrils, Biomacromolecules **18**, 1350 (2017).
[14] J. Guan, F. Vollrath, and D. Porter, Two mechanisms for supercontraction in Nephila spider dragline silk, Biomacromolecules **12**, 4030 (2011).
[15] L. D. Miller, S. Putthanarat, R. Eby, and W. Adams, Investigation of the nanofibrillar morphology in silk fibers by small angle X-ray scattering and atomic force microscopy, International Journal of Biological Macromolecules **24**, 159 (1999).

[16] S. Lin, J. Zhu, X. Li, Y. Guo, Y. Fang, H. Cheng, and H. Zhu, Water-driven actuation of Ornithoctonus huwena spider silk fibers, Appl. Phys. Lett. **110**, 053103 (2017).
[17] D. Sapede, T. Seydel, V. T. Forsyth, M. M. Koza, R. Schweins, F. Vollrath, and C. Riekel, Nanofibrillar structure and molecular mobility in spider dragline silk, Macromolecules **38**, 8447 (2005).
[18] F. Vollrath, T. Holtet, H. C. Thøgersen, and S. Frische, Structural organization of spider silk, Proc. R. Soc. B **263**, 147 (1996).
[19] S. Li, A. McGhie, and S. Tang, New internal structure of spider dragline silk revealed by atomic force microscopy, Biophys. J. **66**, 1209 (1994).
[20] See Supplemental Material at http://link.aps.org/supplemental/10.1103/PhysRevLett.128.098101 for the full derivation of the model and its validation.
[21] M. Elices, G. R. Plaza, J. Perez-Rigueiro, and G. V. Guinea, The hidden link between supercontraction and mechanical behavior of spider silks, J. Mech. Behav. Biomed. Mater. **4**, 658 (2011).
[22] R. W. Work and N. Morosoff, A physico-chemical study of the supercontraction of spider major ampullate silk fibers, Text. Res. J. **52**, 349 (1982).
[23] M. Elices, G. R. Plaza, M. A. Arnedo, J. Perez-Rigueiro, F. G. Torres, and G. V. Guinea, Mechanical behavior of silk during the evolution of orb-web spinning spiders, Biomacromolecules **10**, 1904 (2009).
[24] Y. Liu, Z. Shao, and F. Vollrath, Relationships between supercontraction and mechanical properties of spider silk, Nat. Mater. **4**, 901 (2005).
[25] T. A. Blackledge, C. Boutry, S.-C. Wong, A. Baji, A. Dhinojwala, V. Sahni, and I. Agnarsson, How super is supercontraction? Persistent versus cyclic responses to humidity in spider dragline silk, J. Exp. Biol. **212**, 1981 (2009).
[26] J. M. Gosline, P. A. Guerette, C. S. Ortlepp, and K. N. Savage, The mechanical design of spider silks: From fibroin sequence to mechanical function, J. Exp. Biol. **202**, 3295 (1999).
[27] P. T. Eles and C. A. Michal, Strain dependent local phase transitions observed during controlled supercontraction reveal mechanisms in spider silk, Macromolecules **37**, 1342 (2004).
[28] N. Cohen, M. Levin, and C. D. Eisenbach, On the origin of supercontraction in spider silk, Biomacromolecules **22**, 993 (2021).
[29] D. Liu, A. Tarakanova, C. C. Hsu, M. Yu, S. Zheng, L. Yu, J. Liu, Y. He, D. J. Dunstan, and M. J. Buehler, Spider dragline silk as torsional actuator driven by humidity, Sci. Adv. **5**, eaau9183 (2019).
[30] L. Yu, D. Liu, K. Peng, and Y. He, An improved torsion pendulum based on image processing for single fibers, Meas. Sci. Technol. **27**, 075601 (2016).
[31] D. Liu, L. Yu, Y. He, K. Peng, J. Liu, J. Guan, and D. J. Dunstan, Peculiar torsion dynamical response of spider dragline silk, Appl. Phys. Lett. **111**, 013701 (2017).
[32] G. R. Plaza, G. V. Guinea, J. Perez-Rigueiro, and M. Elices, Thermo-hygro-mechanical behavior of spider dragline silk: Glassy and rubbery states, J. Polym. Sci. Polym. Phys. **44**, 994 (2006).
[33] T. Giesa, R. Schuetz, P. Fratzl, M. J. Buehler, and A. Masic, Unraveling the molecular requirements for macroscopic silk supercontraction, ACS Nano **11**, 9750 (2017).
[34] N. Cohen and C. D. Eisenbach, A microscopically motivated model for the swelling-induced drastic softening of hydrogen-bond dominated biopolymer networks, Acta Biomater. **96**, 303 (2019).
[35] N. Cohen, C. Du, and Z. L. Wu, Understanding the dissociation of hydrogen bond based cross-links in hydrogels due to hydration and mechanical forces, Macromolecules **54**, 11316 (2021).
[36] C. Fu, D. Porter, X. Chen, F. Vollrath, and Z. Shao, Understanding the mechanical properties of antheraea pernyi silk—from primary structure to condensed structure of the protein, Adv. Funct. Mater. **21**, 729 (2011).
[37] D. Porter and F. Vollrath, The role of kinetics of water and amide bonding in protein stability, Soft Matter **4**, 328 (2008).
[38] J. Crank, *The Mathematics of Diffusion* (Oxford University Press, New York, 1979).
[39] I. Agnarsson, C. Boutry, S.-C. Wong, A. Baji, A. Dhinojwala, A. T. Sensenig, and T. A. Blackledge, Supercontraction forces in spider dragline silk depend on hydration rate, Zoology **112**, 325 (2009).
[40] S. Osaki and R. Ishikawa, Determination of elastic modulus of spider's silks, Polym. J. **34**, 25 (2002).
[41] T. Vehoff, A. Glisovic, H. Schollmeyer, A. Zippelius, and T. Salditt, Mechanical properties of spider dragline silk: Humidity, hysteresis, and relaxation, Biophys. J. **93**, 4425 (2007).
[42] S. J. Blamires, C.-P. Liao, C.-K. Chang, Y.-C. Chuang, C.-L. Wu, T. A. Blackledge, H.-S. Sheu, and I.-M. Tso, Mechanical performance of spider silk is robust to nutrient-mediated changes in protein composition, Biomacromolecules **16**, 1218 (2015).
[43] G. G. Kerr, H. F. Nahrung, A. Wiegand, J. Kristoffersen, P. Killen, C. Brown, and J. Macdonald, Mechanical properties of silk of the Australian golden orb weavers Nephila pilipes and Nephila plumipes, Biol. Open **7**, bio029249 (2018).
[44] Z. Wang, Y. Cang, F. Kremer, E. L. Thomas, and G. Fytas, Determination of the complete elasticity of Nephila pilipes spider silk, Biomacromolecules **21**, 1179 (2020).